




Interaction study of Dox-incorporated AS1411 aptamer and nucleolin by molecular dynamics simulation

Paphada Watcharapo, Jiraporn Arunpanichlert, Pichayanoot Rotkrua, Boonchoy Soontornworajit & Yuthana Tantirungrotechai



To cite this article: Paphada Watcharapo, Jiraporn Arunpanichlert, Pichayanoot Rotkrua, Boonchoy Soontornworajit & Yuthana Tantirungrotechai (2023): Interaction study of Dox-incorporated AS1411 aptamer and nucleolin by molecular dynamics simulation, Molecular Simulation, DOI: [10.1080/08927022.2023.2211173](https://doi.org/10.1080/08927022.2023.2211173)

To link to this article: <https://doi.org/10.1080/08927022.2023.2211173>

 View supplementary material 

 Published online: 15 May 2023.

 Submit your article to this journal 

 View related articles 

 View Crossmark data 



Interaction study of Dox-incorporated AS1411 aptamer and nucleolin by molecular dynamics simulation

Paphada Watcharapo^{a,b}, Jiraporn Arunpanichler^{a,b}, Pichayanoot Rotkrua^{b,c}, Boonchoy Soontornworajit^{a,b} and Yuthana Tantirungrotechai^{a,b}

^aDepartment of Chemistry, Faculty of Science and Technology, Thammasat University, Pathumthani, Thailand; ^bThammasat University Research Unit in Innovation of Molecular Hybrid for Biomedical Application, Pathumthani, Thailand; ^cDivision of Biochemistry, Department of Preclinical Science, Faculty of Medicine, Thammasat University, Pathumthani, Thailand

ABSTRACT

AS1411 aptamer is able to recognise the nucleolin overexpressed on cancer cell membranes and has shown promise as a carrier of doxorubicin (Dox) to the cells. This study aimed to study the interaction between nucleolin and aptamers, in either the absence or presence of Dox, using molecular dynamics simulation. AS22nt aptamer was constructed by joining AS1411 aptamer with an additional 22 nucleotide (nt) sequence. NPT simulations were performed from initial docked configuration predicted by HDOCK. The binding of Dox to AS22nt aptamer occurred at the minor groove and the intercalation site in the duplex region. Nucleolin exhibited less flexibility upon binding to AS22nt. The dominant interaction between nucleolin and AS22nt was the electrostatic interaction. The presence of Dox in AS22nt affected the AS22nt-nucleolin interaction contributed by hydrogen bond, hydrophobic contact and ionic interaction. However, the presence of Dox in AS22nt had no impact on the interaction between nucleolin and AS22nt because the magnitudes of binding energy of nucleolin and aptamer with Dox or without Dox were comparable and they were within their calculated deviation. This understanding of nucleolin, AS1411 aptamer, and Dox interactions could provide us a way to prepare an effective targeted anticancer agent for cancer-suffering patients.

ARTICLE HISTORY

Received 22 February 2023
Accepted 27 April 2023

KEYWORDS

AS1411 aptamer; nucleolin; doxorubicin; molecular dynamics simulation

1. Introduction

Chemotherapy drugs such as doxorubicin (Dox) can treat cancers, but they can also cause serious undesirable side effects. A possible solution is to incorporate ligands that recognise cancer-related molecules into a drug delivery system. Aptamers, short oligonucleotides, are attractive ligands because of their low immunogenicity, and their high affinity and specificity to the targets. Aptamers have already been used for drug delivery [1] antiviral [2] and anticancer [3] applications. The AS1411 aptamer binds to nucleolin receptors on cancer cell membranes, and once internalised, it alters the proliferation pathways of the cancer cells [4]. Moreover, the aptamer binding to platelet-derived growth factor BB (PDGF-BB) is used to control the proliferation of cancer cells [5]. Because aptamers are oligonucleotides, they form complex species by base pairing or hybridisation. Anticancer drugs, such as methotrexate and doxorubicin (Dox), can be intercalated in hybridisation regions of aptamers [6,7]. However, more information about binding sites and the molecular interactions is needed to develop effective aptamer-based drug carriers.

Computational approaches are alternative methods for characterising and determining the structural information of a variety of complex systems including biomolecules. Understanding this information can accelerate molecular designs and refinements which benefit biomedical applications [8]. Molecular dynamics (MD) simulation is the most widely

used technique to investigate the characteristics of biomolecules such as protein–ligand interactions. By observing the time-evolution of the system, MD simulation provides dynamical information of molecular phenomena with atomic resolution [9]. A classical MD simulation requires force field parameters to describe the atomic interaction. A number of force field parameters and corresponding MD programs have been developed over the years such as AMBER, CHARMM, GROMACS, and YASARA [9]. An improved version of force field parameters facilitates the applications of MD simulation on novel biomolecule-based systems including the aptamer-based system.

Recently, MD simulation has been applied to study and validate the binding interaction of many nucleic acid aptamers [10]. MD simulation provides evidence of molecular movements affected by the binding interaction. For instance, the structures of retinol-binding protein 4 (RBP4) and the RBP aptamer were determined by UV-visible, circular dichroism (CD) and fluorescence spectroscopy, and their binding mechanism was confirmed by MD simulation. The RBP aptamer was then modified and used to detect RBP4, a promising biomarker for type II diabetes [11]. MD simulation of the streptomycin aptamer revealed that bonding between the antibiotic and the aptamer was spontaneous and that three hydrogen bonds were the dominant interaction [12]. In addition, MD simulations of mucin 1 (MUC1) peptide and an aptamer

revealed that arginine residues in the peptide sequence interacted between the 3' and 5' ends of the aptamer's thymine loop [13]. The AMBER force field accurately describes high charges in the oligonucleotide backbone, the flexibility of the oligomer, and large conformational changes due to external triggers such as metal-ions, temperature, and ligands [14].

As mentioned above, AS1411 aptamer, a G-rich phosphodiester oligonucleotide, specifically binds to nucleolin receptors overexpressed in many cancer cells. This aptamer forms a G-quadruplex structure which facilitates cellular uptakes and increases nuclease resistance; therefore, AS1411 aptamer is a promising molecule for cancer treatment applications. When AS1411 aptamer is internalised into cells, it can stimulate a variety of cell activities including anti-proliferation [15], cell apoptosis [16], and change in cell adhesion [17]. AS1411 can be used as a nanocarrier for MRI contrast agents [18], and it can be tethered to hydroxyapatite nanorods for diagnosis and treatment of cancer [19].

Doxorubicin (Dox) is used to treat various cancers, but it also causes cardiomyopathy and heart failure [20]. This side effect occurs because Dox can nonspecifically induce apoptotic signalling pathways [20], which may result from its redox activation causing the formation of reactive oxygen species (ROS) [21]. To overcome this drawback, targeted drug delivery systems that provide high drug loading efficiency and exhibit low side effects have been developed and applied for cancer treatments [22]. A previous study demonstrated that Dox-dendrimer complex encapsulated in liposomes was able to increase the therapeutic index and reduce the cytotoxicity of the incorporated Dox [23]. In addition, a Dox-loaded *N*-(2-Hydroxypropyl)methacrylamide copolymer showed promise in lowering toxicity of Dox in a target cell [24].

Although AS1411 aptamer is known to recognise nucleolin, which is overexpressed in various cancer cells, molecular details of this interaction have not been well characterised, especially with an intercalated anti-cancer drug. We therefore aimed to investigate the interaction between Dox-incorporated AS1411 aptamer and nucleolin using molecular dynamics simulation. To provide the intercalation site, a sequence of AS1411 aptamer was jointed with an additional 22 nt sequence and named as AS22nt. Then, the interaction in the presence or absence of Dox was monitored. The outcomes could provide an understanding of AS1411 aptamer and nucleolin interaction including the binding sites, the binding affinity, and the dominant type of interaction.

2. Computational methods

2.1. Structure preparation of AS22nt

As the structure of experimental AS22nt was unknown, a model molecule of AS22nt aptamer consisting of G-quadruplex (TTGGTGGTGGTGGTTGTGGTGGTGGTGG) and 22-oligonucleotide (CCATCGGCTATCGAAGCTCGAT) was built using software available on Web servers and YASARA program version 20.7.4.L.64. The structure of G-quadruplex was taken from *Protein Data Bank* (PDB ID: 4U5M). The structure was determined using NMR spectra coupled with the molecular dynamics simulation [25]. The secondary

structure of oligonucleotide was generated by RNAstructure version 6.0.1 (<https://rna.urmc.rochester.edu/RNAstructureWeb/>). The parameters for RNAstructure prediction were temperature of 310.15 K, maximum loop size of 30, maximum percent energy difference of 10, maximum number of predicted structures of 20, window size for maximum free energy prediction of 3, gamma parameter of 1, and minimum helix length of 3. The first ranking structure with the lowest free energy was selected. The secondary structure information was then used to generate an equivalent 3D RNA model with the RNAComposer version 1.0 webserver (<http://rnacomposer.cs.put.poznan.pl>). After that, the 3D RNA structure was converted into a 3D ssDNA structure using Mod-eRNA version 1.7.0 webserver (<http://iimcb.genesilico.pl/modernaserver>). Finally, the 22-oligonucleotide was conjugated to G-quadruplex using YASARA program version 20.7.4.L.64 [26,27]. The conjugation resulted in a phosphodiester bond, a reaction between phosphoric acid and two sugar molecules in the DNA backbone.

2.2. Molecular docking

The Dox-AS22nt aptamer complex docking procedure was performed to predict the favourable binding site using AutoDock 4.2.6 and AutoDockTool 1.5.6 [28]. The Dox molecular coordinate was downloaded from PubChem database (CID 31703). Prior to molecular docking, the receptor and ligand structure pdb files were converted to pdbqt format by AutoDockTools; this step augmented the atom type, polar hydrogen atoms, and united atom Kollman charges required by AutoDock. Then, the search volume was defined around the (8.408, -0.128, -5.715) position with $127 \times 81 \times 67$ grid points (grid spacing = 0.392 Å). All of the single bonds of the Dox were free to rotate, while the aptamer was held rigid. During the Lamarckian genetic algorithm (LGA) search process, a maximum of 50 conformers were considered for each compound with a maximum of 25,000,000 energy evaluations and population size of 300. The structures from the search were ranked according to the interaction energy and were visualised using YASARA.

To understand the binding recognition of AS22nt aptamer on nucleolin, the nucleolin coordinates (PDB ID: 2krr) were retrieved and prepared for protein/RNA docking. All missing residues were reconstructed. Both N-terminal and C-terminal ends of proteins were capped by an acetyl and an N-methyl amide groups, respectively. The protein-aptamer docking was carried out via the HDock web server (<http://hdock.phys.hust.edu.cn>). This server employed a hybrid algorithm to simulate protein-DNA/RNA complexes using template-based modelling and free docking [29]. The nucleolin-AS22nt interaction was presented by docking score and ligand RMSD from this server. Following the prediction of the binding site, the MD simulations were performed using the docked geometries as initial structures.

2.3. MD simulation

The molecular dynamics simulation of all complexes was performed with YASARA program version 20.7.4.L.64. The

complex was placed in the centre of a dodecahedral box with a distance of 10 Å between the complex and each side of the box. Then, the complex was solvated by water molecules with density of 0.997 g/cm³. Sodium and chloride ions were added to the simulation box to neutralise the charge of biomolecules. The system was minimised first to avoid atomic clash, followed by short heating up simulation to 298 K at the pressure of 1 bar. Then, the NPT MD simulation was performed until equilibrium was reached. The production simulation was run for 200 ns using AMBER14 force field [30] for aptamers and nucleolin, GAFF [31] and AM1BCC [32] for Dox, and TIP3P for water. The dodecahedron periodic boundary conditions at a temperature of 298 K and a pressure of 1 bar, and an integration time step of 2 fs were used throughout the simulation.

2.4. Analysis

The trajectory was examined using the YASARA program by taking the starting position as a reference structure. Investigations were conducted on the potential energy, hydrogen bonding, root mean square deviations (RMSD), root mean square fluctuation (RMSF) and B-factor. The Poisson Boltzmann (PBS) method as implemented in YASARA was used to calculate binding energy. This method is similar to MM/PBSA, but it does not have the entropy term from normal mode analysis. The temperature was 298 K and the force field was AMBER14.

3. Results and discussion

3.1. Structural stability of AS22nt

The secondary structure of AS22nt aptamer exhibited G-quadruplex (G4), helical duplex stem (stem) and hairpin loop (loop), as shown in Figure 1(a). The 28nt of AS1411 G4 was conjugated with a 22 nt oligonucleotide by a phosphodiester bond at the C28-C29 segment. Segments A31-A38, A42-C45 and C47-T50 formed base pairing to construct the stem. The loop contained T39-G41, and T46. After that, the molecular dynamics simulation of the AS22nt aptamer was performed for 200 ns. Figure 1(b) shows the total potential energy plot during the simulation. During the first picoseconds, the value of energy rose significantly to reach its equilibrium. The almost constant total potential energy of system indicates that the simulation was stable with the average energy of $-544,390.26 \pm 528.98$ kJ/mol.

To analyse structural stability, the atomic root mean square deviations (RMSDs) of AS22nt were compared to the average structure at after equilibration. The RMSD plot against the simulation time is illustrated in Figure 1(c) and Figure S1. The structure of the AS22nt reached equilibrium after 80 ns. The RMSD value of the whole structure ranged from 2 to 9 Å and the average RMSD value was 4.53 ± 1.46 Å. The RMSD of each individual part reveals the flexibility of each part of AS22nt. The RMSD values of G4, stem, and loop were in the range of 1–7, 2–11 and 2–15 Å, respectively, and the average RMSD values were 3.50 ± 1.19 , 4.75 ± 1.81 , and 6.00 ± 2.25 Å, respectively (Figure 1(d)). The AS1411

quadruplex structure retained its structure while the 22nt tail was flexible, leading to a larger RMSD.

3.2. Effect of Dox on AS22nt structure

The interaction between Dox and AS22nt was investigated by molecular docking and molecular dynamics simulation. Earlier reports suggested that the binding affinity of Dox inside the DNA receptor occurs via either groove interaction or intercalation mechanism [33,34]. We decided to investigate both binding modes. The binding site of minor groove interaction between Dox and AS22nt aptamer, assigned as M-AS22nt, was predicted by AutoDock 4.2.6 and AutoDockTool 1.5.6. AutoDock did not predict the intercalation mode as this requires a large structure change of AS22nt to accommodate the Dox which is not included in the AutoDock model. This has been reported previously [35–37]. For the intercalation study, Dox was initially placed at G-C base pairs of AS22nt using YASARA program and was named I-AS22nt. These two binding modes (Figure 2(a)) were used as initial structures for a 200 ns NPT MD simulation. The average total potential energy of M-AS22nt and I-AS22nt was $-692,008.62 \pm 647.27$ and $-655,1230.50 \pm 637.52$ kJ/mol, respectively (Figure S2). To study the stability of Dox-bound aptamer and validate the docking results [38], RMSDs of M-AS22nt and I-AS22nt were reported in Figure 2(b). All models reached equilibrium after 150 ns. The average RMSD values of M-AS22nt and I-AS22nt were 3.83 ± 1.73 and 4.39 ± 1.10 Å. The RMSD of the ligand from its reference position after receptor superimposition could indicate the accuracy of docking [38]. The average RMSDs of Dox movement in M-AS22nt and I-AS22nt systems were 6.35 ± 3.86 and 3.60 ± 1.17 Å, respectively (Figure S3). This indicated that Dox movement in minor groove interaction played a key role in RMSD fluctuation. Moreover, Dox also exhibited a stable structure because the average RMSD value of Dox with respect to initial Dox structure observed in both systems was 1.39 ± 0.09 and 0.71 ± 0.10 Å (Figure S4). These RMSD results indicated that G4 structure was intact while the major observed conformational changes came from the movement of C29-C30 linker connecting G4 and the 22 nt tail. This part is the most flexible region in the studied molecule.

4. Binding interaction between Dox and AS22nt

The decomposition energy analysis of Dox and AS22nt interaction was performed on the last 50 ns [33,39]. The average number of hydrogen bonds in AS22nt, M-AS22nt and I-AS22nt systems were 49.39 ± 2.77 , 54.36 ± 3.11 and 54.86 ± 2.87 , respectively. Dox formed approximately 3 intermolecular hydrogen bonds with the aptamer and 2 intramolecular hydrogen bonds. This corresponds with the Dox structure that has ketone, amine and hydroxyl groups. We estimated the binding free energy of Dox at the minor groove of AS22nt to be 13.37 ± 38.01 kcal/mol using the PBS method. We would not expect that quantitative result from the PBS method. However, the I-AS22nt system has a binding energy of -19.04 ± 34.92 kcal/mol. The binding energy implies that the binding in the I-AS22nt system is much more stable than that of M-

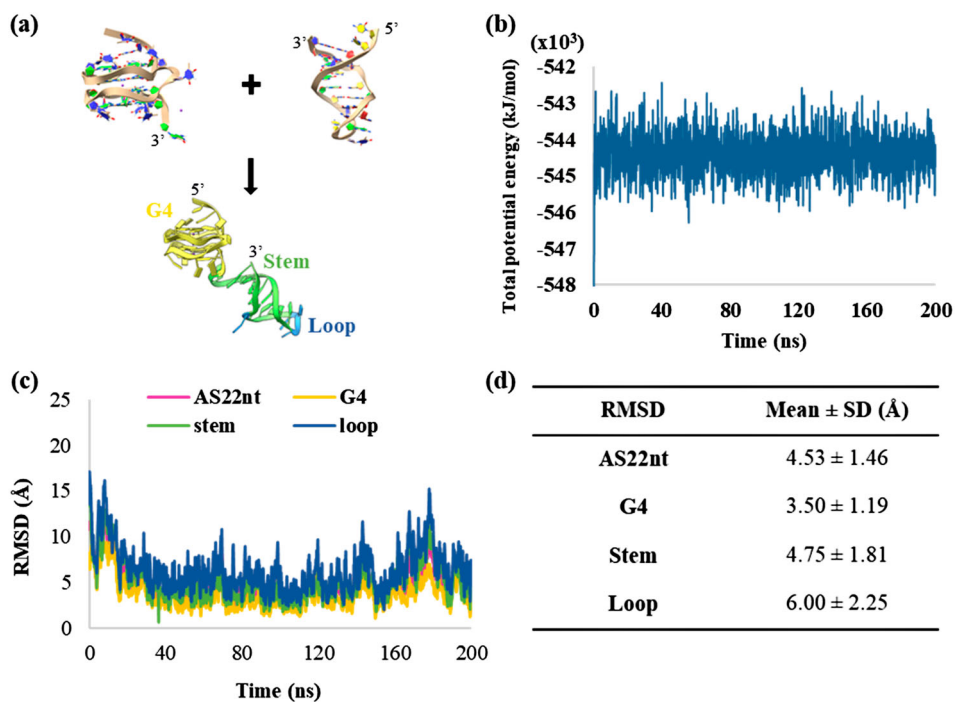


Figure 1 .#(Colour online) Stability of AS22nt aptamer. (a) Structural illustration of AS22nt aptamer generated by YASARA program. (b) Total potential energy of system plotted against simulation time. (c) RMSD of the whole structure and individual regions of AS22nt. (d) Mean and standard deviation values (SD) of RMSD. The average structure once equilibrium is reached at 80 ns is the reference structure.

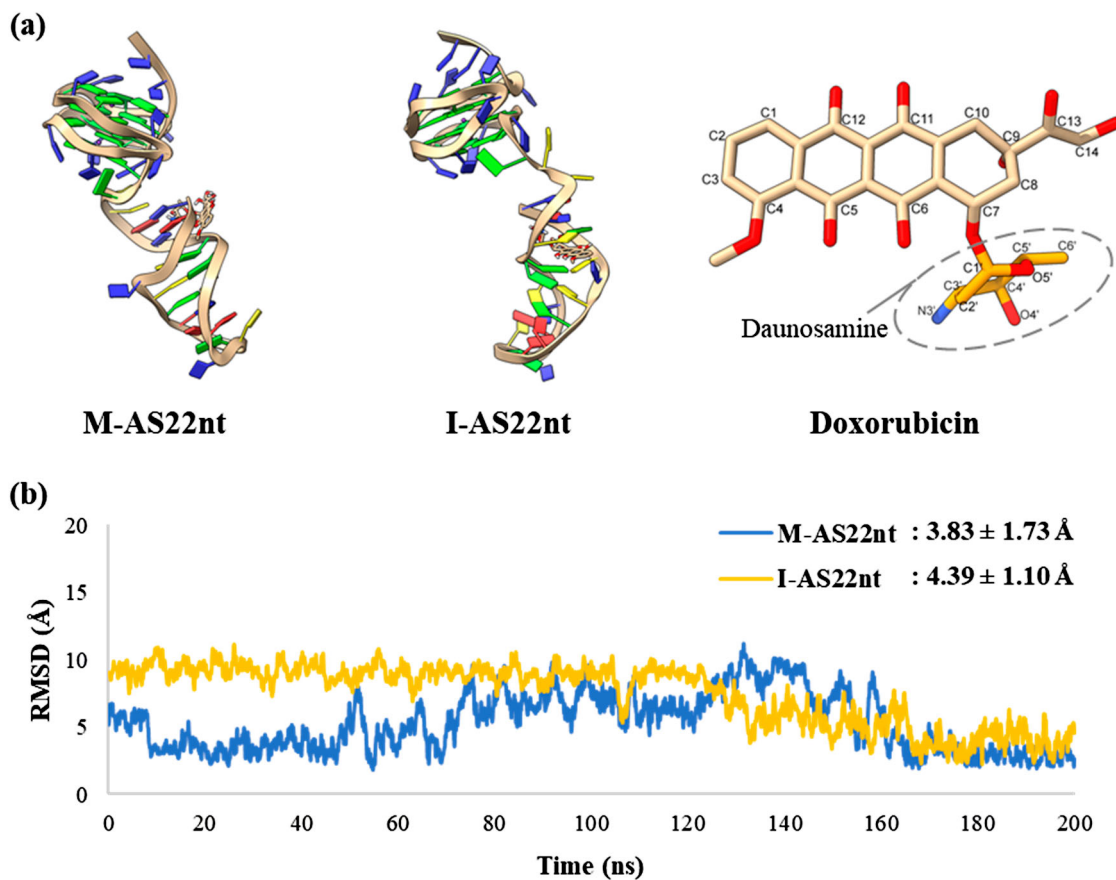


Figure 2 .#(Colour online) Molecular docking of Dox to AS22nt at minor groove and intercalation (a) Structure of M-AS22nt, I-AS22nt and Dox. (b) M-AS22nt and I-AS22nt RMSD values were compared to the average structures of each system retrieved from 150 to 200 ns.

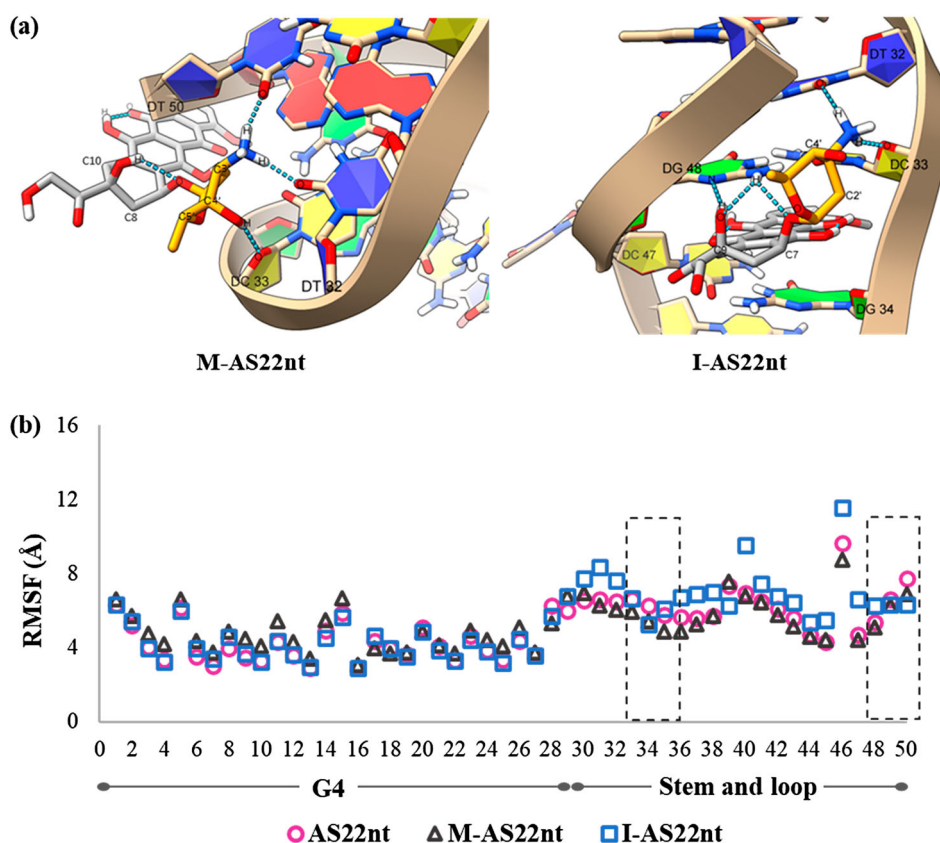


Figure 3 .#(Colour online) Binding interaction between Dox and AS22nt. (a) A 3D binding site of M-AS22nt and I-AS22nt. (b) RMSF values of AS22nt, M-AS22nt and I-AS22nt. Two dash boxes indicate the binding site between Dox and AS22nt.

AS22nt. Details of Dox binding making key contribution of energy calculation were described as follows. Dox was located in proximity to the adenine (A) and thymine (T) base pairs available in the stem part of AS22nt. The NH_2 group in the amino sugar daunosamine of Dox formed a hydrogen bond to oxygen atoms of T32 and T50. Moreover, C33 accepted a polar hydrogen atom from an oxygen atom at C4' of the daunosamine group of Dox. The results of M-AS22nt indicated that daunosamine acts as a minor groove binder, which confirmed an earlier theoretical work of Shevchuk *et al.* [40]. The relative free energy in both complexes indicated that Dox was stable in the intercalation site. The Dox was surrounded by C33 and G48 base pairs of AS22nt. Hydrogen bonds were observed between the following pairs of atoms: oxygen of T32...H-N of daunosamine, oxygen of C33...H-N of daunosamine, oxygen of C7 of aglycone...polar hydrogen of G48, and OH at C9 of aglycone...H-N of G48. As the calculated binding energy of the M-AS22nt system is positive with a large deviation, it may be inconclusive to assume that the binding process is endergonic. From the trajectory and the observed binding mode, one would however be certain that the interaction is only weak, due to the Dox fluctuation at the minor groove binding site. Moreover, the Dox is more strongly bound to the G-C base pair than to the A-T base pair of the AS22nt aptamer.

The effect of Dox on aptamer flexibility was characterised by the RMSF of nucleotides, as shown in Figure 3. For all systems, the RMSF values of G4 were generally lower than that of stem and loop. This agrees with the rigidity of the G4 unit

compared to the flexible stem and loop parts. The interaction of AS22nt with Dox had nucleotides from residues T32, C33 and G48 to T50 located at the stem (Figure 3(a)). At those key binding residues, the RMSF of M-AS22nt was comparable to that of AS22nt, while the RMSF of I-AS22nt deviated slightly from that of AS22nt as it had lower magnitudes. This indicated that the binding residues of I-AS22nt were less flexible than other two systems. An interesting phenomenon was found in the loop region (T39-G41, and T46). This loop region in I-AS22nt was more flexible than that in AS22nt and M-AS22nt. This might be due to a strong interaction of Dox at the intercalation sites which had more constraints while the adjacent nucleotides had more freedom of movement. Meanwhile, the loop region in M-AS22nt was as flexible as that in AS22nt indicating weak interaction of Dox in the minor groove system. RMSFs of these binding site residues in I-AS22nt were lower than that in AS22nt, as highlighted in dashed rectangular boxes (Figure 3(b)). These results indicated that Dox interaction caused the reduction in the flexibility of the structure in stem regions.

4.1. Investigation of nucleolin-AS22nt interaction

To investigate the interaction of nucleolin and AS22nt, the complex of nucleolin-AS22nt was formed and served as a model. Before protein-ligand binding simulation, the conformational change of nucleolin was investigated. To verify the structural stability of nucleolin, the total potential energy, as shown in Figure S5, and RMSD, as shown in Figure 4(b),

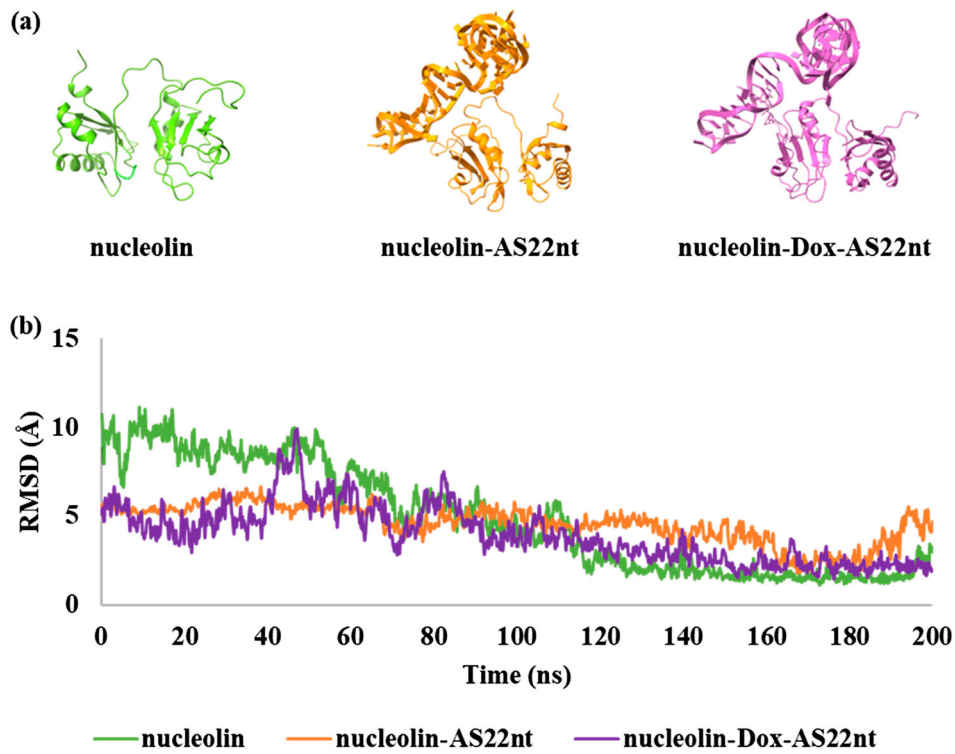


Figure 4 .#(Colour online) Investigation of nucleolin-AS22nt interaction. (a) A 3D structure of nucleolin, nucleolin-AS22nt complex and nucleolin-Dox-AS22nt complex. (b) RMSD of nucleolin, nucleolin-AS22nt complex and nucleolin-Dox-AS22nt complex. The average structure of each system after equilibration is used as the reference structure for RMSD analysis of nucleolin, nucleolin-AS22nt, and nucleolin-Dox-AS22nt systems.

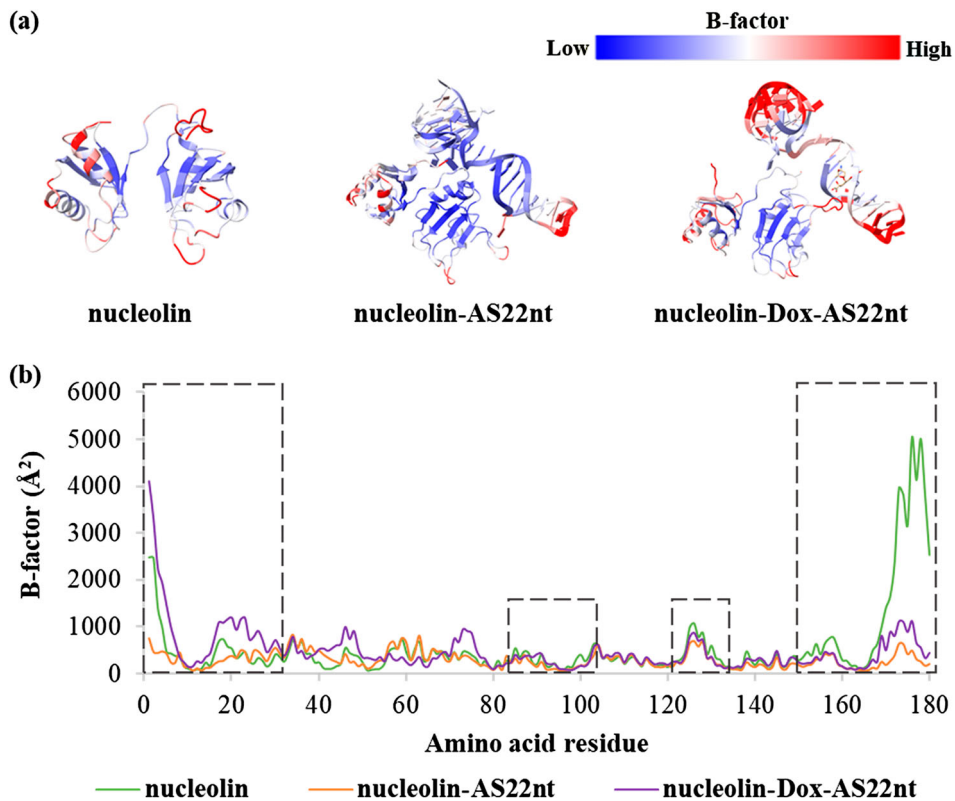


Figure 5 .#(Colour online) The flexibility of nucleolin. (a) The scale bar indicated colours ranging from blue (rigid) to red (flexible). (b) B-factor of nucleolin, nucleolin-AS22nt complex and nucleolin-Dox-AS22nt complex. Dashed rectangular boxes illustrated the location of binding sites.

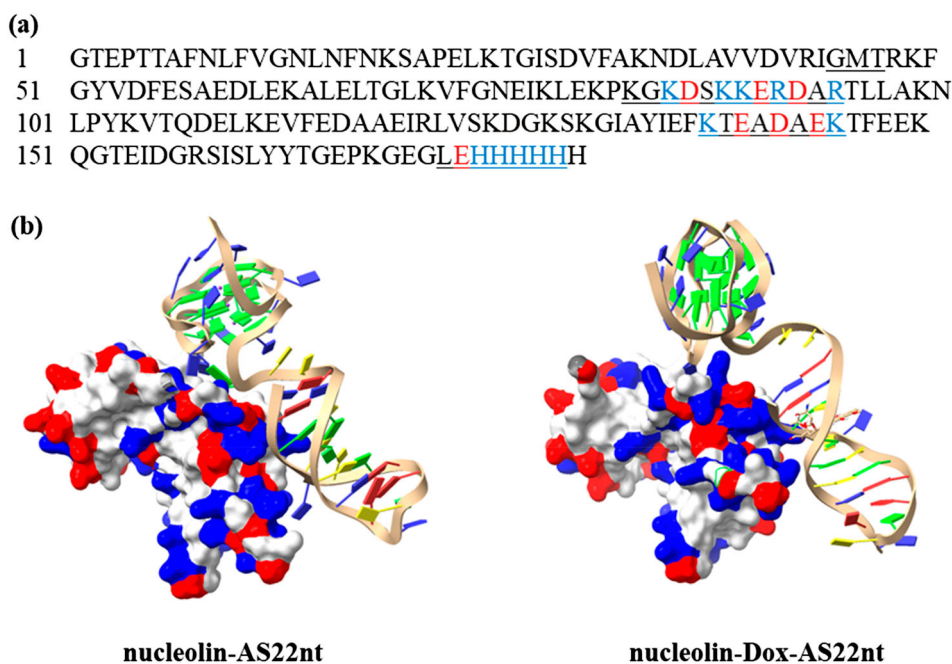


Figure 6 .#(Colour online) (a) The sequence indicated the amino acid sequence alignment of nucleolin. (b) The 3-D surface structure of the AS22nt binding domain of nucleolin. Amino acids with negative and positive charges are coloured red and blue, respectively.

were measured. The average total potential energy of the nucleolin system was $-335,740.06 \pm 469.31$ kJ/mol. The average RMSD value of nucleolin after 150 ns was 1.70 ± 0.38 Å. The results indicated that the lower the fluctuation of total potential energy and RMSD, the more stable nucleolin structure. Then, the binding site of the AS22nt, in the presence or absence of Dox, and nucleolin was predicted on the HDock web server. The assembled models were clustered with RMSD cutoff of 5 Å, and ranked according to a docking score, indicating a probable binding model. These docked structures served as the initial structure for MD simulation. As discussed earlier, Dox intercalation exhibited a more stable complex, therefore the following observation was based on Dox intercalation model (I-AS22nt). The models of nucleolin-AS22nt and nucleolin-Dox-AS22nt complex are shown in Figure 4(a). The MD analysis of two models was carried out for 200 ns and RMSD of each system was monitored (Figure 4(b)). The RMSD of nucleolin-AS22nt and nucleolin-Dox-AS22nt complex after 150 ns were 3.25 ± 1.94 Å and 2.21 ± 0.39 Å. These RMSD values were in the same order of magnitude and they were comparable. This hinted to us that Dox had no role in nucleolin-aptamer binding interaction. In addition, the interaction between nucleolin and this aptamer sequence was governed by its G-quadruplex structure, the number of nucleotide strands, polarity of nucleotide strands, and cations [41]. In addition, the cations that make a contribution to G-quadruplex stability were either K^+ , Na^+ , Rb^+ , Cs^+ , NH_4^+ , or Tl^+ [41]. K^+ was the most effective one since it lowered negative electrostatic potential energy, effectively [41,42].

4.2. The flexibility of nucleolin

To understand the flexibility of each residue upon forming the complex, the B-factor of nucleolin was evaluated; it was

visualised with colours ranging from blue (lowest or rigid) to red (highest or flexible) in Figure 5(a). The B-factors per amino acid residue of models are shown in a plot in Figure 5(b) with the dashed rectangular boxes representing residues in the vicinity of the AS22nt system, indicating the rigidity of this segment. However, other regions are coloured blue to red, indicating flexible regions. Therefore, it suggested that the flexibility of structure in nucleolin was decreased due to interaction between this molecule and AS22nt with either Dox intercalation.

4.3. Prediction of nucleolin-AS22nt binding site

To investigate the binding site of nucleolin and AS22nt, the predicted structure from HDock was used as the initial structure of nucleolin-AS22nt complex. The nucleolin-AS22nt complex and the nucleolin-Dox-AS22nt complex demonstrated that nucleolin interacted with both G-quadruplex and 22nt tail of AS22nt aptamer. To understand the molecular detail of interaction in complexes, Figure 6(a) shows the nucleolin sequence with the underlined sequence highlighting the amino acids that bind the aptamer. In addition, the docking conformation of complexes is shown in Figure 6(b), which indicates amino acid residues interact with AS22nt. The majority residues of nucleolin that interacted with AS22nt were Lys83, Lys85, Ser87, Lys88, Lys89, Glu90, Arg91, Arg94, Lys138, Thr139, Ala141, Glu144, Leu173, His175, His176 and His178. Most of these residues were positively charged, such as lysine (Lys, K), arginine (Arg, R) and histidine (His, H), while aspartic acid (Asp, D) and glutamic acid (Glu, E) were negatively charged. Therefore, the dominant nucleolin/aptamer interaction is believed to be the electrostatic interaction between the positively charged amino acid residues and the negatively charged phosphate groups in the aptamer.

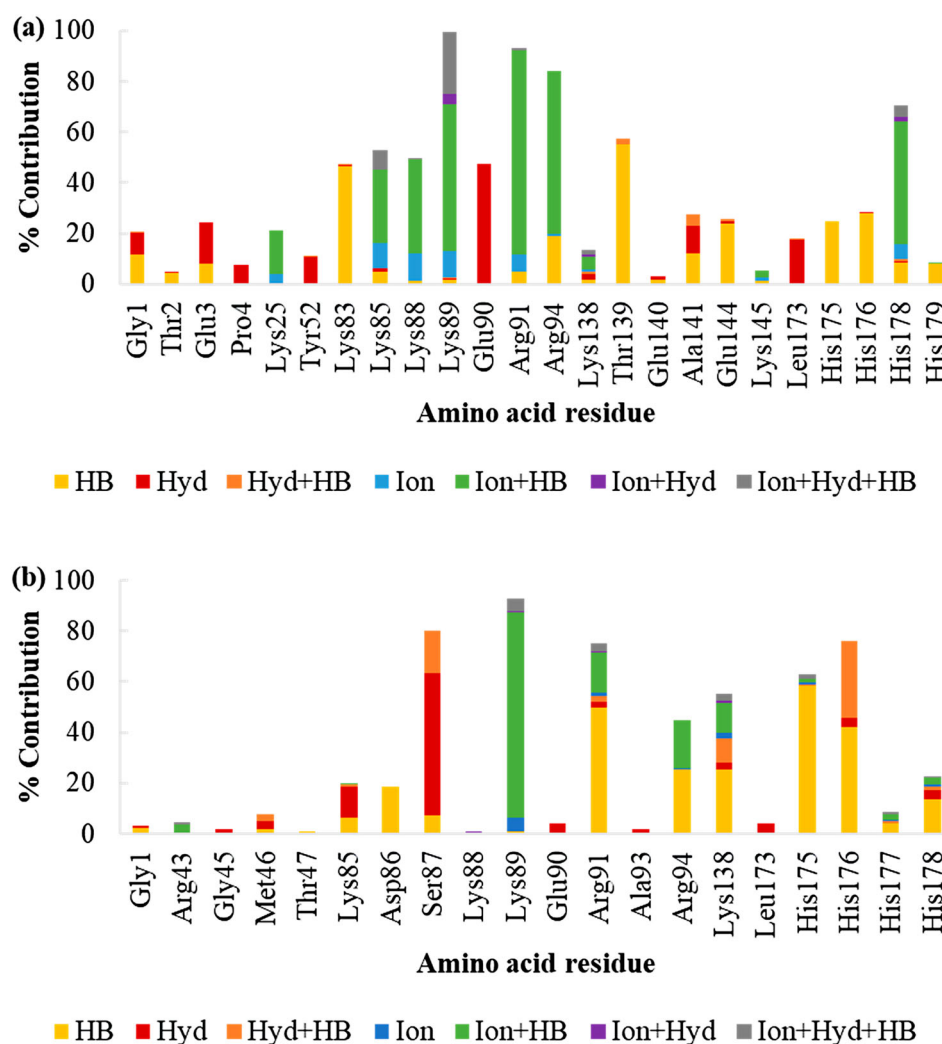


Figure 7. (Colour online) The interaction of the major residue pairwise in a binding site in nucleolin and AS22nt. The average number of various types of interactions of (a) nucleolin with AS22nt and (b) nucleolin with Dox-AS22nt. Types of interaction are shown as hydrogen bond (HB), hydrophobic contact (Hyd) and ionic interaction (Ion).

In order to gain insight into the interaction between nucleolin and AS22nt, the average number of various types of interactions was divided into each residue. The three different types of interactions are hydrogen bonds (HB), hydrophobic contacts (Hyd), and ionic interactions (ion). Mixtures of these interactions may contribute if a residue takes part in more than one type of interaction with AS22nt (Figure 7). As mentioned in the above investigation, the major residues that interact with AS22nt have positively charged atoms, indicating ionic interactions. Meanwhile, alanine (Ala, A) and leucine (Leu, L) are hydrophobic residues, causing hydrophobic interaction with AS22nt. This nonpolar interaction plays an essential role in the specificity and strong affinity [43]. Moreover, hydrogen bonding is a key component in a specific recognition, due to the fact that both nucleic acids and amino acids have hydrogen donor-acceptor potentials [44]. These results indicated that the binding interaction between nucleolin and AS22nt involved hydrogen bonds, ionic interaction, and hydrophobic interaction, which enhanced the protein-DNA binding. Additionally, the PBS method in the YASARA program was used to analyse the binding energies of nucleolin-

AS22nt and nucleolin-Dox-AS22nt. The average binding energy from the last 50 ns for nucleolin-AS22nt, and nucleolin-Dox-AS22nt was 110.78 ± 58.60 , and 119.29 ± 60.16 kcal/mol, respectively. These binding energy values were in the same order of magnitude and within the same uncertainty level. This binding energy analysis revealed that Dox intercalation sites were in a position that had no effect on the interaction between nucleolin and the studied aptamer. This finding supported that AS22nt was able to carry Dox and deliver this drug into cells as reported in previous studies [45,46].

5. Conclusion

Within this work, we have performed computational studies to evaluate the predictive binding characteristics of AS22nt and Dox-AS22nt against the nucleolin commonly found in cancer cells. AS22nt was allowed to reach its equilibrium as demonstrated by total potential energy, RMSD, and RMSF. Additionally, the interaction between Dox and AS22nt governed by minor groove binding and intercalation was investigated. The analysis of free energy demonstrated that Dox

intercalation yielded a more stable and rigid complex than the minor groove binding. The intercalation was found to have taken place at cytosine and guanine bases in the DNA duplex. The binding interaction between AS22nt and nucleolin was investigated using MD simulation, yielding insight into the binding conformation, including binding stability. Investigation of residue fluctuations showed that the flexibility of nucleolin was decreased due to the binding interaction with AS22nt and Dox-AS2nt. Binding energy indicated that Dox played no role in nucleolin-aptamer interaction. This suggests the role of AS22nt aptamer as a Dox carrier towards nucleolin. Moreover, per-residue analysis indicated that residue binding sites were facilitated by hydrogen bonds, ionic interactions, and hydrophobic interactions. The major contribution came from electrostatic interactions between positively charged amino acids and negatively charged phosphate groups in the DNA backbone. These understandings of the interaction between AS1411 aptamer, Dox, and nucleolin would be invaluable information for further biomedical applications which could enhance our well-being.

Acknowledgements

The authors gratefully acknowledge the financial support provided by Thammasat University Research Unit in Innovation of Molecular Hybrid for Biomedical Application. The authors thank Mr. Michael Jan Everts, Clinical Research Center, Faculty of Medicine, Thammasat University, for comments on the manuscript.

Disclosure statement

No potential conflict of interest was reported by the author(s).

Funding

This work was supported by Thammasat University Research Unit in Innovation of Molecular Hybrid for Biomedical Application, Thammasat University.

Data availability statement

All data are available from the corresponding author on reasonable request.

References

- [1] Zhan Y, Ma W, Zhang Y, et al. DNA-based nanomedicine with targeting and enhancement of therapeutic efficacy of breast cancer cells. *ACS Appl Mater Interf.* 2019;11(17):15354–15365.
- [2] Chen S, Cai G, Gong X, et al. Non-autofluorescence detection of H5N1 virus using photochemical aptamer sensors based on persistent luminescent nanoparticles. *ACS Appl Mater Interf.* 2022;14(41):46964–46971.
- [3] Riccardi C, Napolitano E, Platella C, et al. Anti-VEGF DNA-based aptamers in cancer therapeutics and diagnostics. *Med Res Rev.* 2021;41(1):464–506.
- [4] Reyes-Reyes EM, Teng Y, Bates PJ. A new paradigm for aptamer therapeutic AS1411 action: uptake by macropinocytosis and its stimulation by a nucleolin-dependent mechanism. *Cancer Res.* 2010;70(21):8617–8629.
- [5] Lu, C, Shahzad MMK, Myrthala M-S, et al. Targeting pericytes with a PDGF-B aptamer in human ovarian. *Cancer Biol Ther.* 2010;9(3):176–182.
- [6] Agudelo D, Bourassa P, Berube G, et al. Review on the binding of anticancer drug doxorubicin with DNA and tRNA: structural models and antitumor activity. *J Photochem Photobiol B-Biol.* 2016;158:274–279.
- [7] Pontinha ADR, Jorge SMA, Paquim AMC, et al. In situ evaluation of anticancer drug methotrexate-DNA interaction using a DNA-electrochemical biosensor and AFM characterization. *Phys Chem Chem Phys.* 2011;13(12):5227–5234.
- [8] Akram N, Mansha A, Premkumar R, et al. Spectroscopic, quantum chemical and molecular docking studies on 2,4-dimethoxy-1,3,5-triazine: a potent inhibitor of protein kinase CK2 for the development of breast cancer drug. *Mol Simul.* 2020;46(17):1340–1353.
- [9] Norberg J, Nilsson L. Advances in biomolecular simulations: methodology and recent applications. *Q Rev Biophys.* 2003;36:257–306.
- [10] Kumar N, Seminario JM. Molecular dynamics study of thrombin capture by aptamers TBA26 and TBA29 coupled to a DNA origami. *Mol Simul.* 2018;44(9):749–756.
- [11] Torabi R, Bagherzadeh K, Ghourchian H, et al. An investigation on the interaction modes of a single-strand DNA aptamer and RBP4 protein: a molecular dynamic simulations approach. *Org Biomol Chem.* 2016;14(34):8141–8153.
- [12] Nick TA, de Oliveira TE, Pilat DW, et al. Stability of a split streptomycin binding aptamer. *J Phys Chem B.* 2016;120(27):6479–6489.
- [13] Rhinehardt KL, Srinivas G, Mohan RV. Molecular dynamics simulation analysis of anti-MUC1 aptamer and mucin 1 peptide binding. *J Phys Chem B.* 2015;119(22):6571–6583.
- [14] Albada HB, Golub E, Willner I. Computational docking simulations of a DNA-aptamer for argininamide and related ligands. *J Comput Aided Mol Des.* 2015;29(7):643–654.
- [15] Cheng Y, Zhao G, Zhang SW, et al. AS1411-induced growth inhibition of glioma cells by up-regulation of p53 and down-regulation of Bcl-2 and Akt1 via nucleolin. *PLoS One.* 2016;11(12):20.
- [16] Sharma VR, Thomas SD, Miller DM, et al. Nucleolin overexpression confers increased sensitivity to the anti-nucleolin aptamer, AS1411. *Cancer Invest.* 2018;36(9–10):475–491.
- [17] Feng LY, Li W, Ren JS, et al. Electrochemically and DNA-triggered cell release from ferrocene/beta-cyclodextrin and aptamer modified dual-functionalized graphene substrate. *Nano Res.* 2015;8(3):887–899.
- [18] Zhang KC, Liu M, Tong XY, et al. Aptamer-modified temperature-sensitive liposomal contrast agent for magnetic resonance imaging. *Biomacromolecules.* 2015;16(9):2618–2623.
- [19] Li ZH, Liu Z, Yin ML, et al. Aptamer-capped multifunctional mesoporous strontium hydroxyapatite nanovehicle for cancer-cell-responsive drug delivery and imaging. *Biomacromolecules.* 2012;13(12):4257–4263.
- [20] Singal PK, Iliskovic N. Doxorubicin-induced cardiomyopathy. *N Engl J Med.* 1998;339(13):900–905.
- [21] Sawyer DB, Fukazawa R, Arstall MA, et al. Daunorubicin-induced apoptosis in rat cardiac myocytes is inhibited by dexrazoxane. *Circ Res.* 1999;84(3):257–265.
- [22] Bagalkot V, Farokhzad OC, Langer R, et al. An aptamer-doxorubicin physical conjugate as a novel targeted drug-delivery platform. *Angew Chem Int Ed.* 2006;45(48):8149–8152.
- [23] Papiagiannaros A, Dimas K, Papaioannou GT, et al. Doxorubicin-PAMAM dendrimer complex attached to liposomes: cytotoxic studies against human cancer cell lines. *Int J Pharm.* 2005;302(1–2):29–38.
- [24] Wang D, Kopečková P, Minko T, et al. Synthesis of starlike N-(2-hydroxypropyl)methacrylamide copolymers: potential drug carriers. *Biomacromolecules.* 2000;1(3):313–319.
- [25] Chung WJ, Heddi B, Schmitt E, et al. Structure of a left-handed DNA G-quadruplex. *Proc Natl Acad Sci.* 2015;112(9):2729–2733.
- [26] Krieger E, Nabuurs SB, Vriend G. Homology modeling. *Methods Biochem Anal.* 2003;44:509–524.

- [27] Dash R, Ali MC, Dash N, et al. Structural and dynamic characterizations highlight the deleterious role of SULT1A1 R213H polymorphism in substrate binding. *Int J Mol Sci.* 2019;20:6256.
- [28] Trott O, Olson A. Software news and update AutoDock Vina: improving the speed and accuracy of docking with a new scoring function, efficient optimization, and multithreading. *J Comput Chem.* 2010;31:455–461.
- [29] Yan Y, Zhang D, Zhou P, et al. HDOCK: a web server for protein–protein and protein–DNA/RNA docking based on a hybrid strategy. *Nucleic Acids Res.* 2017;45(W1):W365–W373.
- [30] Dickson CJ, Madej BD, Skjevik ÅA, et al. Lipid14: the amber lipid force field. *J Chem Theory Comput.* 2014;10(2):865–879.
- [31] Wang J, Wolf R, Caldwell J, et al. Development and testing of a general AMBER force field. *J Comput Chem.* 2004;25:1157–1174.
- [32] Jakalian A, Jack D, Bayly C. Fast, efficient generation of high quality atomic charges. AM1–BCC model: II. Parameterization and validation. *J Comput Chem.* 2002;23:1623–1641.
- [33] Hassani Moghadam F, Taher MA, Karimi-Maleh H. Doxorubicin anticancer drug monitoring by ds-DNA-based electrochemical biosensor in clinical samples. *Micromachines.* 2021;12:808.
- [34] Ijäs H, Shen B, Heuer-Jungemann A, et al. Unraveling the interaction between doxorubicin and DNA origami nanostructures for customizable chemotherapeutic drug release. *Nucleic Acids Res.* 2021;49(6):3048–3062.
- [35] Jawad B, Poudel L, Podgornik R, et al. Thermodynamic dissection of the intercalation binding process of doxorubicin to dsDNA with implications of ionic and solvent effects. *J Phys Chem B.* 2020;124(36):7803–7818.
- [36] Hu Q, Li H, Wang L, et al. DNA nanotechnology-enabled drug delivery systems. *Chem Rev.* 2019;119(10):6459–6506.
- [37] Mondal S, Samajdar RN, Mukherjee S, et al. Unique features of metformin: a combined experimental, theoretical, and simulation study of its structure, dynamics, and interaction energetics with DNA grooves. *J Phys Chem B.* 2018;122(8):2227–2242.
- [38] Bell EW, Zhang Y. DockRMSD: an open-source tool for atom mapping and RMSD calculation of symmetric molecules through graph isomorphism. *J Cheminformatics.* 2019;11(1):40.
- [39] Reddy K, Wang Y. Understanding co-loading and releasing of doxorubicin and paclitaxel using chitosan functionalized single-walled carbon nanotubes by molecular dynamics simulations. *Phys Chem Chem Phys.* 2018;20:9389–9400.
- [40] Shevchuk O, Posokhova E, Sakhno L, et al. Theoretical ground for adsorptive therapy of anthracyclines cardiotoxicity. *Exp Oncol.* 2012;34:314–322.
- [41] Yuan WF, Wan LY, Peng H, et al. The influencing factors and functions of DNA G-quadruplexes. *Cell Biochem Funct.* 2020;38(5):524–532.
- [42] Hud NV, Smith FW, Anet FAL, et al. The selectivity for K⁺ versus Na⁺ in DNA quadruplexes is dominated by relative free energies of hydration: a thermodynamic analysis by 1H NMR. *Biochemistry.* 1996;35(48):15383–15390.
- [43] Bie L, Wang Y, Jiang F, et al. Insights into the binding mode of AS1411 aptamer to nucleolin. *Front Mol Biosci.* 2022. doi:10.3389/fmolb.2022.1025313.
- [44] Matsushita Y, Murakawa T, Shimamura K, et al. Change in specific interactions between lactose repressor protein and DNA induced by ligand binding: molecular dynamics and molecular orbital calculations. *Molecular Simulation.* 2016;42(3):242–256.
- [45] Liao Z-X, Chuang E-Y, Lin C-C, et al. An AS1411 aptamer-conjugated liposomal system containing a bubble-generating agent for tumor-specific chemotherapy that overcomes multidrug resistance. *J Control Release Off J Control Release Soc.* 2015;208:42–51.
- [46] Rotkrua P, Lohlamoh W, Watcharapo P, et al. A molecular hybrid comprising AS1411 and PDGF-BB aptamer, cholesterol, and doxorubicin for inhibiting proliferation of SW480 cells. *J Mol Recognit.* 2021;34:e2926.